RSC Advances

ROYAL SOCIETY OF CHEMISTRY

www.rsc.org/advances

Journal Name

ARTICLE

Preparation of porous 3D Ce-doped ZnO microflowers with enhanced photocatalytic performance

Received 00th January 20xx,
Accepted 00th January 20xx

DOI: 10.1039/x0xx00000x

www.rsc.org/

Yimai Liang[a], Na Guo[a], Linlin Li[a], Ruiqing Li[a], Guijuan Ji[a]* and Shucai Gan[a]*

Porous 3D Ce-doped ZnO microflowers were prepared by hydrothermal method followed by low annealing process. The effects of Ce doping on the structural and photocatalytic properties of porous ZnO microflowers were investigated in detail. The samples were characterized by XRD, SEM, EDS, XPS, DRS, PL spectrum and BET surface area measurements. According to XRD analysis, both the crystalline structure of the synthesized pure ZnO and Ce-doped ZnO samples are hexagonal wurtzite. XPS results demonstrated that successfully synthesis of Ce^{4+} doped ZnO. In addition, SEM morphologies showed the unique porous 3D flower-like structure of Ce-doped ZnO. Compared with the porous ZnO microflowers, the Ce-doped ZnO samples exhibit improved photocatalytic performance on decompose Rhodamine B (RhB). It is proposed that the special structural feature with a porous 3D structured and Ce modification lead to the rapid photocatalytic activity of the Ce-doped ZnO microflowers.

1. Introduction

Environment pollution is one of the main problems and challenges that human beings have to face in contemporary society, and many basic and applied researches on environmental remediation have been carried out, especially photocatalysts of wide band gap semiconductors.[1, 2] The semiconductor photocatalysts, as environmentally friendly catalysts, have potential ability to remove the contaminations in air and water without causing additive damage to our environment.[3–5] Under light irradiation, pollutant could be decomposed into non-toxic substance on the surface of photocatalyst. ZnO, a wide-direct band gap (3.37 eV) metal-oxide semiconductor, is a promising photocatalytic material owing to its low cost, excellent catalytic efficiency, high physical and chemical stability, and environmental sustainability.[6] Additionally, the ZnO photocatalyst can be easily manipulated with desirable micro and nanoscale structures, which are proved to be important factors affecting the photocatalytic activity. Among numerous structures, the 3D porous structure of ZnO has attracted tremendous interest due to superior photocatalytic properties as compared with various low-dimensional ZnO structures.[7-9] Such special structure not only avoid the self-aggregation of small particles, but also make larger surface area and provide more active sites during the reaction, facilitating the diffusion and mass transportation of organic molecules and increasing the photocatalytic reaction rate.[10]

However, the rapid recombination of photogenerated electron–hole pairs formed in photocatalytic processes is a major obstacle for increasing the photocatalytic efficiency of ZnO.[11] To solve this problem, one of the efficient methods is the modification of semiconductors with electron scavenging agents, such as noble metals,[12-14] metal oxides,[15, 16] carbon materials[17, 18] and so on. Recently, there are some reports that using some dopants that can act as trapping sites to retard the electron-hole recombination rate and increase the photocatalytic activity.[19, 20] Among a variety of dopants, rare-earth doped ZnO materials have potential applications in many technologies such as degradation of pollutants and optoelectronic devices.[21, 22] Cerium is a major element in the useful rare earth family. Some attention has been paid to synthesis the Ce-doped zinc oxide for the applications in various technologies. Li *et al*. synthesized Ce-doped ZnO hollow nanofibers via facile single capillary electrospinning and performed gas sensing properties.[23] Rezaei *et al*. prepared Ce-doped ZnO nanoparticles in water by refluxing for 3 h about at 90 ^{o}C and applied for photodegradation reaction.[24] Jung *et al*. studied optical properties of Ce-doped ZnO nanorods fabricated in hydrothermal method on a Si (100) substrate.[25] Although there are a few reports about Ce-doped ZnO materials which have been successfully synthesized, there is little literature reported for the fabrication of the architectures of porous 3D flower-like Ce-doped ZnO composites and the study its photocatalytic properties.

In the present research, we prepared porous 3D Ce-doped ZnO microflowers using low temperature-hydrothermal method followed by a heat treatment process for the first time. The effects of cerium doping on the structural and optical properties of ZnO microflowers were also investigated in detail. Finally, the photocatalytic activity of as-prepared

[a]College of Chemistry, Jilin University, Changchun 130026, P.R. China.
*Corresponding authors: Guijuan Ji; Shucai Gan
E-mail address: juanziji@126.com (G. Ji); gansc@jlu.edu.cn (S. Gan).
Tel: +86 431 88502259.

composites is studied, and a possible mechanism of photocatalysis is also discussed and proposed.

2. Experimental section

2.1 Chemicals

All reagents, including zinc nitrate hexahydrate ($Zn(NO_3)_2{\cdot}6H_2O$, AR), hexamethylenetetramine (HMT, AR), cerium nitrate hexahydrate ($Ce(NO_3)_3{\cdot}6H_2O$, 99.95%) and oxalic acid dehydrate ($H_2C_2O_4{\cdot}2H_2O$, AR) were purchased from Beijing Chemical Reagent Research Company and Shanghai Aladdin Industrial Corporation. Distilled water was used for all experimental processes.

2.2 Synthesis of porous 3D Ce-doped ZnO microflowers

3 mmol $Zn(NO_3)_2{\cdot}6H_2O$, 3 mmol HMT and different amounts of $Ce(NO_3)_3{\cdot}6H_2O$ were dissolved in 80 mL distilled water. After being stirred for 15 min., then 0.3 mmol $H_2C_2O_4{\cdot}2H_2O$ were added into the above solution. Then additional agitation for 30 min., the mixture was transferred to a 100 mL Teflon-line autoclave and sealed. The autoclave was heated up to 90 ^{o}C and maintained at this temperature for 3 h. After naturally cooling down to room temperature, the resulting precipitates were collected by centrifugation, washed three times with distilled water and ethanol and then dried at 70 ^{o}C in air for 12 h. The samples were retrieved through a heat treatment of the precursors at 400 ^{o}C in air for 1h with a heating rate of 1 ^{o}C min^{-1}. A various of porous 3D Ce-doped ZnO microflowers composites were prepared by adding different molar concentrations of $Ce(NO_3)_3{\cdot}6H_2O$ to the $Zn(NO_3)_2{\cdot}6H_2O$ precursor. The molar ratio of $Ce(NO_3)_3{\cdot}6H_2O/Zn(NO_3)_2{\cdot}6H_2O$ was changed in the range from 0 to 5% and the samples were denoted as ZnO, CZ-0.25%, CZ-0.5%, CZ-1%, CZ-3% and CZ-5% respectively, in which the last number corresponds to the molar ratio of $Ce(NO_3)_3{\cdot}6H_2O/Zn(NO_3)_2{\cdot}6H_2O$.

2.3. Characterization

The crystallographic structures of the porous 3D Ce-doped ZnO microflowers were collected by powders X-ray diffraction using a D/Max-IIIC (Rigaku, Japan) with Cu Kα radiation. The morphology and dimension of as-synthesized microstructures were carried out by S-4800 field emission scanning electron microscope (FE-SEM, Hitachi, Japan) equipped with an energy-dispersive X-ray spectrometer (EDX, JEOL JXA-840). X-ray photoelectron spectroscopy (XPS) analysis was performed on a PHI-5000CESCA system with Mg K radiation (hv = 1253.6 eV). The X-ray anode was run at 250 W, and the high voltage was kept at 14.0 kV with a detection angle at 540^{o}. All the binding energies were calibrated by using the containment carbon (C 1s = 284.6 eV). The Brunauer–Emmett–Teller (BET) surface area of the powders was analyzed by nitrogen adsorption on a Micromeritics ASAP 2020 nitrogen adsorption apparatus (U.S.A.). The sample was degassed in vacuum at 150 ^{o}C for 7 h before nitrogen adsorption measurement. The BET surface area was determined by a multipoint BET method using the adsorption data in the relative pressure (P/P_0) range of 0.01–0.99. Adsorption branches of the isotherms were used to determine the pore size distributions for the samples studied via the Barrett–Joyner–Halenda (BJH) method. The volume of nitrogen adsorbed at the relative pressure (P/P_0) of 0.99 was used to determine the pore volume. The photoluminescence spectra (PL) of porous 3D Ce-doped ZnO microflowers were recorded using a Hitachi F-7000 spectrophotometer equipped with a 150 W xenon lamp at 341 nm excitation wavelength. All measurements were performed at room temperature.

2.4 Photocatalytic experiments

The photocatalytic activity of the as-prepared samples was evaluated by using RhB as targeted dye pollutant. A high-pressure Hg UV lamp (GGZ175, 175 W) with a maximum emission at 365 nm served as UV light resource. In a typical procedure, 0.04 g catalyst was dispersed into 20 mL aqueous solution of RhB (8 mg L^{-1}). After stirring in the dark for 30 min, the suspensions were placed under UV-light irradiation. Finishing the photoreaction, the samples were collected at regular intervals and centrifuged to remove the catalyst. The concentration of target organic solution before and after degradation was measured by using a UV–vis spectrometer (UV-2550, Shimadzu, Japan).

3. Results and discussion

3.1. Morphological and structural analysis

The phase characteristics of the synthetic samples were performed by powder X-ray diffraction (XRD). Fig. 1 shows the XRD patterns of the porous 3D ZnO microflowers and Ce-doped ZnO microflowers with different amount of cerium ions, respectively. For pure ZnO, the diffraction peaks are consistent with (100), (002), (101), (102), (110), (103), (200), (112), (201), and (202) planes in agreement with wurtzite hexagonal crystalline phase of ZnO (JCPDS No. 36-1451). The sharp diffraction peak showed in the XRD patterns illuminate that ZnO were highly crystallized. However, for Ce-doped ZnO, with the increasing of doping concentration, the intensity of diffraction peaks decrease, the crystalline quality of ZnO degrades, suggesting that the increasing of doping concentration deteriorated the crystal structure of ZnO. Similar dopant-induced changes in crystallization have been observed in nickel-doped ZnO.[26] We also found that, for a lower concentration of Ce-doping no other crystalline impurities were detected in the XRD pattern. This may be due to the fact that at low concentrations of cerium ions, these ions would uniformly substitute Zn^{2+} sites or interstitial sites in ZnO lattice.[27] However at higher concentrations of Ce doping (3% and 5%), a small peak located at about 2θ = 28.4° attributed to (111) reflection plane of CeO_2 show up. Similar behavior of cerium doped ZnO nanocrystals was reported by Kannadasan *et al*.[28]

Fig. 2a and b demonstrates the SEM images of the synthesized CZ-1% sample. As is shown in Fig. 2a, the CZ-1% exhibits a well-defined 3D morphology which resembled a peony flower pattern. The detailed observation of a single CZ-1% microflower is shown in Fig. 2b, the entire flower-like structure is assembled by numerous porous nanoplates with an average thickness of ~15 nm. It can be found that these nanosheets intersect with each other and result in flower-like structures. In addition, we can obviously observe that there

are numerous pores in the nanoplates, which are shown in the inset of Fig. 2b. The large amount of the nanopores in the nanosheets should be beneficial to enlarge the contact area for enhanced reactant diffusivity, which is highly favorable for catalytic activity.[29] The EDS analysis was done and the result is mentioned in Fig. 2c. In the EDS spectrum, numerous well-defined peaks were evident related to Zn, O and Ce which clearly support that the synthesized the CZ-1% is composed of Zn, O and Ce. No other peak related to impurities was detected in the spectrum which further confirms that Ce-doped ZnO was successfully synthesized.

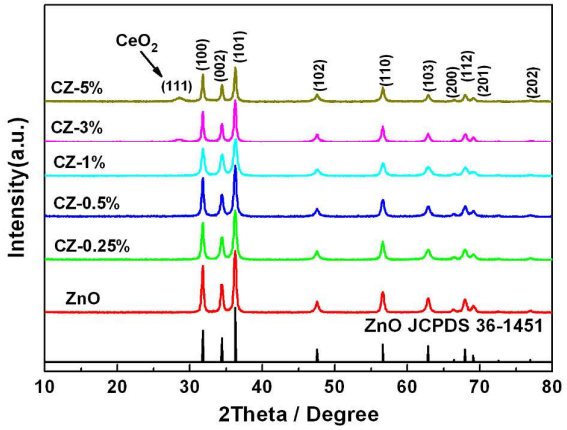

Fig. 1. XRD patterns of ZnO and Ce-doped ZnO.

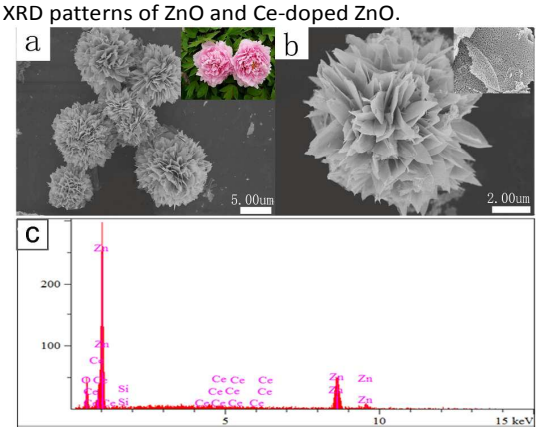

Fig. 2. SEM (a, b) and EDS (c) patterns of the porous flower-like CZ-1% sample.

To further assess the effect of Ce doped amount on the morphology. Fig. 3 shows the SEM micrographs of the as prepared products with different Ce doped concentrations, respectively. As can be seen from the Fig. 3a, the undoped ZnO is composed of 3D flower-like structures with a smooth surface. It is clearly that the damage degree of product morphology is smaller when Ce doping concentration is lower. ZnO remains a flower like structure basically with Ce doping concentration is 3% (Fig. 3b-e). With the incorporation of Ce ions into the ZnO, the flower-like structure partly broke up and morphology became rougher. When the doping concentration is 5% (Fig. 3f), some branches of the flower like aggregate decrease, the nanosheets of hierarchical porous microflowers became severely damaged. This phenomenon is more obvious, and the reason is that the Ce ionic radius is larger than Zn ionic, Ce can replace the Zn ion when it enters into the lattice of ZnO and may damage the crystal structure. The greater the proportion of Ce ions entering the ZnO lattice, the more Zn ions are replaced by Ce. Therefore ZnO original crystal structure is destroyed gradually.[30]

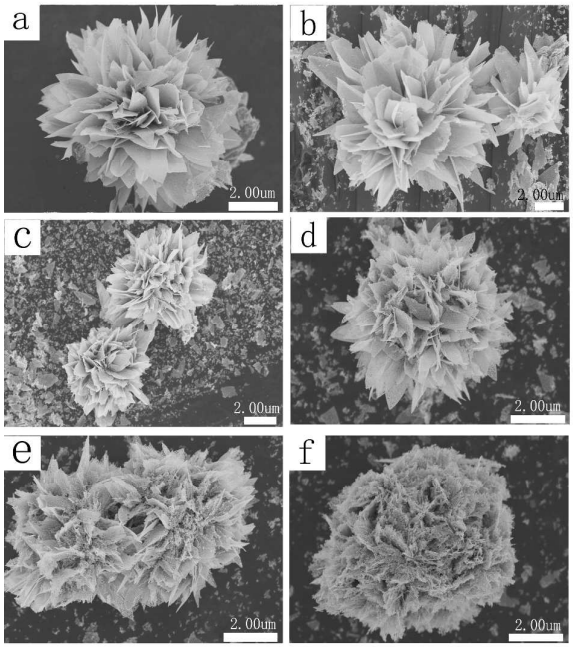

Fig. 3. SEM pattern for (a) undoped ZnO , (b) CZ-0.25%, (c) CZ-0.5%, (d) CZ-1%, (e) CZ-3%, and (f) CZ-5%.

3.2. XPS analysis

In order to determine the surface composition and chemical state of the sample, CZ-1% was studied by XPS technique. The survey result in Fig. 4a demonstrates that all peaks are ascribed to Zn, Ce, O and C (due to air contamination and CO/CO_2 adsorption on the surface), which confirming CZ-1% is composed of three elements of Zn, Ce and O. The results are in good agreement with XRD and EDS as described above. The high-resolution scans Zn 2p, Ce 3d, and O 1s has been carried out. As can be seen from Fig. 4b, the XPS spectrum of Zn 2p gives peak centered at 1021.8 eV (Zn 2p3/2) and 1044.6 eV (Zn 2p1/2) respectively, which are similar to that of pure ZnO, this finding confirms that Zn exists mainly in the Zn^{2+} chemical state on the sample surface.[31] In Fig. 4c, the O 1s profile can be fitted to two peaks, indicating that two different kinds of O species existed in the sample. The peaks are attributed to the crystal lattice oxygen in ZnO (locating at 530.2 eV) and the adsorbed oxygen on the catalyst surface (locating at 531.5 eV), respectively.[32] In the Ce 3d spectrum (Fig. 4d), six peaks corresponding to three pairs of spin–orbit doublets could be identified as the Ce 3d5/2 (v_0, v_1, v_2) and Ce 3d3/2 (v_0' v_1', v_2'), which clearly indicates that the Ce ions have a +4 oxidation valance state.[33] The high binding energy doublet v_2, v_2' at

898.9 and 916.5 eV are originated from the final state of Ce (IV) $3d^9 4f^0 O2p^6$, doublet v_1, v_1' at 888.7 and 907.5 eV are attributed to the state of Ce (IV) $3d^9 4f^1 O2p^5$, and doublet v_0, v_0' at 882.5 and 901.7 eV are corresponding to the state of Ce (IV) $3d^9 4f^2 O2p^4$. All this confirmed that the samples were doped with cerium in the form of Ce(IV).[34] Besides, these values of Ce 3d binding energy for the Ce-doped ZnO microflowers slightly shifted compared with standard XPS energy peak locations of Ce 3d.[35] The slight shift indicates that the Ce–O bond length in ZnO has changed due to Ce^{4+} doped on the ZnO sample, which is similar to ZnO: Tb thin films.[36] In addition, no signals of other impurities are detected from the Fig. 4, implying the synthesis of Ce^{4+}-doped ZnO microflowers.

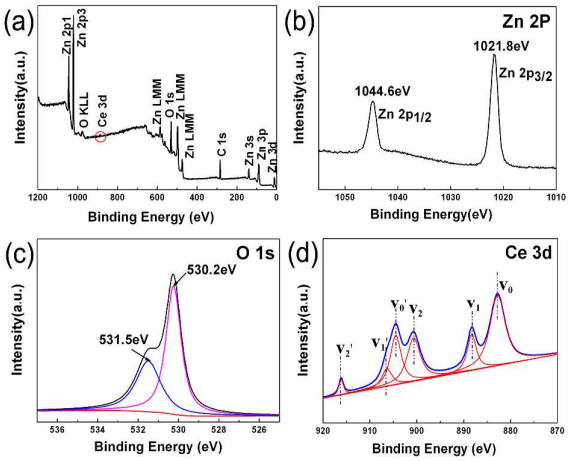

Fig. 4. XPS spectra of the porous CZ-1% microflower (a) XPS full spectra of the samples, the high resolution scans of (b) Zn 2p, O 1s and (d) Ce 3d.

3.3. BET surface measurements

To investigate the specific areas and the porous nature of the ZnO and Ce-doped ZnO microflowers, Brunauer-Emmett-Teller (BET) gassorption measurements were performed. The nitrogen adsorption/desorption isotherms and the pore size distribution plots of the porous flower-like ZnO and CZ-1% samples are shown in Fig. 5. All the samples display the type IV curve accompanied by a type H3 hysteresis loop, which is attributed to the predominance of mesopores, according to the IUPAC classification.[37] The pore size distributions of the ZnO and CZ-1% are given in the inset of Fig. 5. The samples have a bimodal pore distribution using the Barrett-Joyner-Halenda (BJH) method. Clearly, the smaller-sized pores are intrinsic within the nanoplates of ZnO and CZ-1%, whereas the larger-sized pores are mainly due to interstices between the nanoplates.[38] In addition, the BET surface area, pore size and crystal size of all the samples are summarized in Table 1. It can be seen that the specific surface area of Ce-doped ZnO is higher than the native ZnO. This increase in surface area can be attributed to the decrease of the crystal size of the nanoparticles. By applying the Scherrer formula for the broadening of (101) peak reflection of ZnO, the crystal sizes of pure ZnO and Ce-doped ZnO with different Ce doped concentrations samples were found to be 23.4, 19.2, 18.1, 15.6, 22.2, and 21.1 nm (shown in Table 1), respectively, indicating that doping with Ce creates surface defect sites and surface disorder, and had a depression effect on the growth of crystal size. Systematically when the Ce concentrations were increased from 0 to 1%, the specific surface area increased, which might be due to the decrease in the crystallite size. However, the specific surface area decreased when the Ce concentration was further increased to 3%. This might be due to the structure of the porous microflowers was damaged, and these particles aggregate increasing the crystallite size. It can be consisted with the results of SEM. Thus, it is evident that the cerium amount influences significantly the surface area of photocatalysts, which our conclusion can be supported by literature.[39-41]

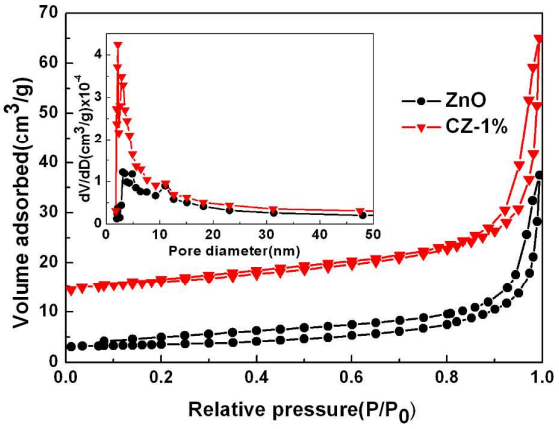

Fig. 5. N_2 adsorption/desorption isotherms and BJH pore diameter distribution of the porous ZnO and CZ-1% microflowers.

Table 1 BET surface area of porous flower-like ZnO and Ce-doped ZnO with different Ce doped concentrations.

Samples	Surface area (m^2/g)	Pore size (nm)	Crystal size (nm)
ZnO	10.47	18.62	23.4
CZ-0.25%	11.30	20.53	19.2
CZ-0.5%	12.10	15.19	18.1
CZ-1%	21.07	16.15	15.6
CZ-3%	13.44	17.22	22.2
CZ-5%	16.62	16.20	21.1

3.4. UV–vis diffuse reflectance and photoluminescence spectrum

Diffuse reflectance UV–visible spectra of undoped ZnO and Ce-doped ZnO samples at different Ce contents (0.25%, 0.5%, 1%, 3% and 5%) are presented in Fig. 6. The strong absorption in the UV region (200–400 nm) is assigned to ZnO. It can be seen that the pristine ZnO possesses the most light absorption between 200-400nm. This indicate that our uniform 3D microstructure of ZnO having excellent light trapping characteristics. Both the hierarchical organized structure itself and the voids between and within the nanosheets are advantageous for enhanced light absorption due to reflection of trapped incident light within the samples, [7, 8] and the

hierarchical ZnO microflower ensure a large specific surface which is favorable for enhancing the light absorption and the light propagation; as confirmed by the SEM and BET surface area results. Undoped porous ZnO microflowers had no absorption in the visible region (>400 nm). However, the Ce-doped ZnO microflowers exhibited a broad absorption tail band between 400 and 500 nm. By comparing ZnO with Ce-doped ZnO, it can still be found that the doping leads to noticeable red-shift in the absorption band in visible light region. The reason may attribute to appearance of a new electronic state among the ZnO band-gap. The distance of charge transfer between f electrons of the cerium ions and the conduction band (CB) or valence band (VB) of ZnO is narrowed, thus allowing visible light absorption. When the doping amount of Ce is increased from 0 to 1%, the absorbance intensity of the Ce-doped ZnO microflowers increased in visible light region. It due to the fact that the Ce doped into the ZnO crystal grains can greatly increase the visible light absorption ability. When the doping concentration increased to 3% and 5%, the visible light absorption ability of the Ce-doped ZnO is decreased. As we know, doping is usually accompanied by the formation of defects, which can play the role as trap centers to photoelectrons, but excessive doping may lead to some surface defects to act as the recombination centers for electron hole and thus decrease the photocatalytic activity. Similar optical spectra were observed by some previous literatures. [42, 43] It reveals that the Ce-doped ZnO microflowers may have photocatalytic properties under sunlight irradiation.[44-46] Besides, the optical absorption of Ce-doped ZnO microflowers in the UV region was enhanced. The band gap value of the samples is calculated by the formula Eg (eV) = 1240/λg (nm), where λg stands for the wavelength value corresponding to the intersection point of the vertical and horizontal parts of the spectra, and a narrowing of the band gap value is observed with an increase in cerium content (3.06 eV for ZnO, 3.04 eV for CZ-0.25%, 3.01 eV for CZ-0.5%, 2.98 eV for CZ-1%, 2.96 eV for CZ-3%, and 2.93 eV for CZ-5%).

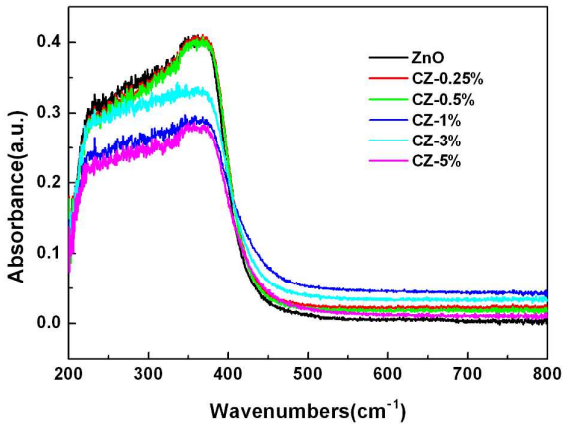

Fig. 6. UV–vis diffuse reflectance spectra of porous 3D ZnO and Ce-doped ZnO with various Ce contents.

The Photoluminescence (PL) spectra of undoped and Ce-doped ZnO samples were evaluated to observe the electronic structure and fate of electrons and holes separations.[47] The PL is excited at a wavelength of 334 nm. The excitation wavelength was determined from the absorption spectra. As seen in Fig. 7, two types of major emission peaks were observed i.e. one sharp peak near UV region and a broad peak in visible light region. The sharp UV emission can be ascribed to the near-band-edge emission of ZnO originating from electron–hole recombination.[48, 49] It is worth to note that the PL spectra of Ce-doped ZnO shows a decrease as compared to the pure ZnO in the intensity of UV emission peak, which indicates the reduction of the recombination centers for the electrons and holes in the samples when doping Ce on ZnO. Moreover, it can be seen clearly that the sample CZ-1% shows the minimum PL intensity. When the amount of the Ce increased further up to 3%, the intensity of the spectra was increased, and indicates that the recombination of the electrons and holes was increased. The increase of the recombination of electrons and holes can be attributed the surface defects created by the excess dopant, which acts as recombination centers, and consequently, increased the charge recombination.[50] The charge separation and recombination impose a direct impact on the photocatalytic activity of the catalyst. According to the above analysis, it can be seen that doping Ce can make the intensity of PL decrease. The weaker is PL response, the better is the separation efficiency of photoinduced electron–hole pairs, and the higher will be the photocatalytic performance of Ce-doped ZnO composites, which will be discussed in Section 3.5.

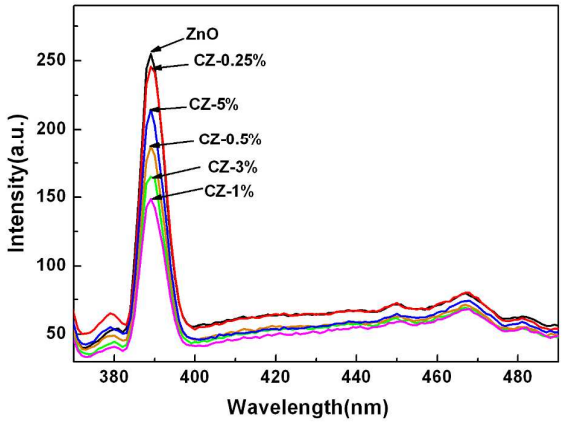

Fig. 7. PL spectra of porous 3D ZnO and Ce-doped ZnO with various Ce doped.

3.5. Photocatalytic performance

The photocatalytic degradation of RhB has been chosen as a representative reaction to evaluate the photocatalytic activities of the as-synthesized Ce-doped ZnO under UV irradiation. As a contrast, the degradation curves of RhB by undoped ZnO and the blank experiment (without any catalyst added) were also presented. As shown in Fig. 8, there is only a little decrease of RhB concentration in blank experiment after UV irradiation for 120 min, indicating that the photolysis of RhB solution with the blank is negligible in our experimental

conditions. The porous Ce-doped ZnO catalysts exhibit higher photocatalytic activities compared to undoped ZnO microflowers, indicating the Ce-dopant played a significant role. Furthermore, the photocatalytic efficiency varied with the amount of Ce in the samples, and the CZ-1% exhibited the highest photocatalytic activity, which was also corroborated by the PL behavior. When the Ce amount increases from 0.25% to 1%, there is more of the dominant Ce^{4+} to capture electrons, resulting in a greater photocatalytic activity. But, if the amount of Ce^{4+} ions is higher than the optimum amount (x > 1%), the high concentration of dopant ions act as recombination centers of electrons and holes and hence the photocatalytic activity decreases.[51] The photocatalytic degradation of RhB can be considered as a pseudo-first-order reaction. The efficiency of RhB photodegradation by the photocatalyst was determined quantitatively using the pseudo-first-order model as follow: $\ln(C/C_0) = -kt$, where C_0 and C are the concentrations of dye at time 0 and t respectively and k is the apparent rate constant (min^{-1}). The pseudo-first-order rate constants k of the various photocatalysts was shown in Table 2. The results clearly demonstrate that the CZ-1% sample shows the highest catalytic activity with rate constant k = 1.2173 min^{-1} that is about 2 times higher than that of pure ZnO (0.6520 min^{-1}). These results show that the photocatalytic activity of ZnO can be obviously improved in the presence of Ce-dopant.

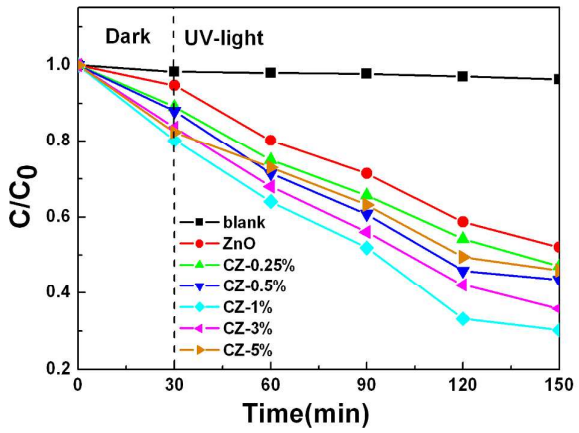

Fig. 8. Photodegradation curves of RhB by different catalysts under UV-light irradiation.

Table 2 The apparent rate constant k calculated for different catalyst systems.

Photocatalysts	Kinetic constants k (min^{-1})
blank	0.0021
ZnO	0.6520
CZ-0.25%	0.7529
CZ-0.5%	0.8951
CZ-1%	1.2173
CZ-3%	1.0210
CZ-5%	0.7881

3.6. Photocatalytic mechanism

A mechanistic scheme diagram of the charge separation and photocatalytic reaction for Ce-doped ZnO photocatalyst is shown in Fig. 9. For the undoped ZnO, the photocatalyst were irradiated by UV-light, electrons (e^-) in the valence band (VB) were excited to the conduction band (CB) with the generation of holes (h^+) in the VB (Eq. (1)). Generally, these electron–holes recombine quickly, leading to a decrease in catalytic activity of ZnO. For Ce-doped ZnO, the Ce 4f level has crucial influences on the photo-excited charge generation and transfer, together with the inhibition of electron–hole recombination. Ce^{4+} could act as an effective electron scavenger to trap the conduction band (CB) electrons of Ce-doped ZnO photocatalysts. Ce^{4+} acts as stronger Lewis acid than O_2. Ce^{4+} ion is superior to O_2 in its capability of trapping electrons (Eq. (2)). The electrons can transfer to the adsorbed O_2 by an oxidation process (Eq. (3)), and produce a superoxide radical anion ($\cdot O_2^-$).[52] Meanwhile, the photoinduced holes in ZnO can be also readily scavenged by the immanence H_2O molecules to yield ·OH radicals (Eq. (4)). The highly reactive superoxide radical anion ($\cdot O_2^-$) and hydroxyl radical (·OH) are responsible for the degradation of the organic chemicals, which can be destroyed into mineral acids, CO_2 and H_2O (Eq. (5, 6)).This process can be proposed as follows.[53]

$$ZnO + h\nu \rightarrow e^- + h^+ \quad (1)$$

$$Ce^{4+} + e^- \rightarrow Ce^{3+} \quad (2)$$

$$Ce^{3+} + O_2 \rightarrow Ce^{4+} + \bullet O_2^- \quad (3)$$

$$h^+ + H_2O \rightarrow \bullet OH + H^+ \quad (4)$$

$$RhB + \bullet O_2^- \rightarrow \text{Mineral acids} + CO_2 + H_2O \quad (5)$$

$$RhB + \bullet OH \rightarrow \text{Mineral acids} + CO_2 + H_2O \quad (6)$$

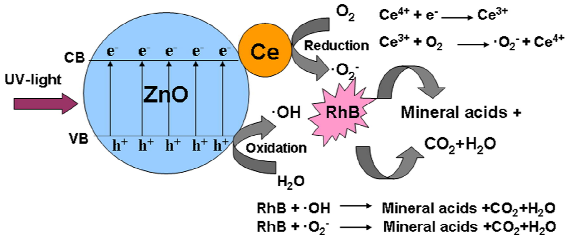

Fig. 9. UV-light-induced charge separation and photocatalytic mechanism of the porous Ce-doped ZnO.

4. Conclusions

In summary, we successfully synthesized the porous 3D Ce-doped ZnO microflowers with hydrothermal method followed by a heat treatment for the first time. The influence of cerium dopant on the structural and photocatalytic properties of the

synthesized porous ZnO microflowers samples has been investigated in detail. According to the XPS analysis revealed that the cerium doped ZnO microflowers contain mainly Ce^{4+} ions. The BET surface measurements showed an increase in the specific surface area of the samples after the incorporation of Ce^{4+}. All Ce-doped samples showed a significantly higher photocatalytic activity as compared to the pure porous ZnO for the degradation of RhB. Moreover, the CZ-1% microflower exhibits highest photocatalytic activity among the prepared samples. Ce, with a moderate amount doped on ZnO, can act as electron trap and suppresses the photogenerated electrons–hole pair recombination and results in the improvement of photocatalytic performance samples. The PL spectra reveal the inhibition of recombination of the photogenerated electrons and holes pairs by the samples, which is consistent with the photocatalytic performance results.

Acknowledgements

This work was supported by Mineral and Ore Resources Comprehensive Utilization of Advanced Technology Popularization and Practical Research (MORCUATPPR) founded by the China Geological Survey (grant no. 12120113088300). It was also supported by Key Technology and Equipment of Efficient Utilization of Oil Shale Resources (no. OSR-05) and the National Science and Technology Major Projects (no. 2008ZX05018).

References

1 G. Palmisano, V. Auguliaro, M. Pagliaro and L. Palmisano, *Chem. Commun.* 2007, **33**, 3425–3437.
2 C. G. Tian, Q. Zhang, A. P. Wu, M. J. Jiang and Z. L. Liang, *Chem. Commun*. 2012, **48**, 2858–2860.
3 A. A. Abdel-Wahab and A. M. Gaber, *J. Photochem. Photobiol. A: Chem.* 1998, **114**, 205–210.
4 M. Raula and M. Biswas, *RSC Adv*. 2014, **4**, 5055–5064.
5 T. Gotoh, K. Matsushima and K. L. Kikuchi, *Chemosphere.* 2004, **55**, 135–140.
6 B. Jeong, D. H. Kim, E. J. Park, M. G. Jeong and K. Dae, *Appl. Surf. Sci*. 2014, **307**, 468–474.
7 Z. D. Li, Y. Zhou, G. G. Xue, T. Yu and J. G. Liu, *J. Mater. Chem*. 2012, **22**, 14341–14345.
8 W. L. Ong, S. Natarajan, B. Kloostra and G. W. Ho, *Nanoscale*. 2013, **5**, 5568–5575.
9 Z. J. Xing, B. Y. Geng, X. L. Li, H. Jiang and C. X. Feng, *CrystEngComm*. 2011, **13**, 2137–2142.
10 S. W. Liu, C. Li, J. G. Yu and Q. J Xiang, *CrystEngComm*. 2011, **13**, 2533–2541.
11 Y. M. Liang, N. Guo, L. L. Li, R. Q. Li, G. J. Ji and S. C. Gan, *Appl. Surf. Sci*. 2015, **332**, 32–39.
12 Z. C. Wu, C. G. Xu, Y. Q. Wu and F. Gao, *CrystEngComm*. 2013, **15**, 5994–6002.
13 H. B. Zeng, W. P. Cai, P. S. Liu, X. X. Xu, H. J. Zhou, C. Klingshirn and H. Kalt, *ACS Nano*. 2008, **2**, 1661–1670.
14 C. L. Yu, K. Yang, Y. Xie, Q. Z. Fan and C. Y. Wang, *Nanoscale*. 2013, **5**, 2142–2151.
15 X. Huang, L. Shang, S. Chen, J. Xia, X. P. Qi and X. C. Wang, *Nanoscale*. 2013, **5**, 3828–3833.
16 S. Khanchandani, S. Kundu, A. Patra and A.K. Ganguli, *J. Phys. Chem. C.* 2012, **116**, 23653–23662.
17 R. J. Zou, G. J. He, K. B. Xu, Q. Liu and J. Q. Hu, *J. Mater. Chem. A*. 2013, **1**, 8445–8452.
18 A. S. Alshammari, L. N. Chi, X. P. Chen, A. Bagabas and Z. Jiang, *RSC Adv*. 2015, **5**, 27690–27698.
19 F. Ahmed, S. Kumar, N. Arshi, M. S. Anwar and B. H. Koo, *CrystEngComm*. 2012, **14**, 4016–4026.
20 S. Kuriakose, B. Satpatib and S. Mohapatra, *Phys. Chem. Chem. Phys*. 2014, **16**, 12741–12749.
21 T. M. Williams, D. Hunter and A. K. Pradhan, *Appl. Phys. Lett*. 2006, **89**, 43116–43119.
22 Y. Jiang, Y. Liu, L. Yang, and J. Liu. *Adv. Mater. Res.* 2012, **490**, 3262–3265.
23 W. Q. Li, S. Y. Ma, G. J. Yang and Y. Z. Mao, *Mater. Lett.* 2015, **138**, 188–191.
24 M. Rezaei and A. Habibi-Yangjeh, *Appl. Surf. Sci.* 2013, **265**, 591–596.
25 Y. Jung, B. Young and Y. S. Lee, *Nanoscale. Res. Lett.* 2012, **7**, 43.
26 N. V. Kaneva, D. T. Dimitrov and C. D. Dushkin. *Appl. Surf. Sci*. 2011, **257**, 8113–8120.
27 M. Faisal , Adel A. Ismail and Ahmed A. Ibrahim, *Chem. Eng. J*. 2013, **229**, 225–233.
28 N. Kannadasan, N. Shanmugam, S. Cholan, K. Sathishkumar, G. Viruthagiri and R. Poonguzhali, *Mater. Charact.* 2014, **97**, 37–46.
29 L. F. Koao, F. B. Dejene, H. C. Swart , J. R. Botha, *J. Lumin*. 2013, **143**, 463–468.
30 Z. F. Wang, Y. H. Zhang and J. Mao, *Adv. Mater. Res.* 2014, **834**, 12–17.
31 Y. H. Zheng, L. R. Zheng, Y. Y. Zhan, X .Y. Lin, Q. Zheng and K. M. Wei, *Inorg. Chem.* 2007, **46**, 6980–6986.
32 H. W. Bai, Z. Y. Liu and D. D. Sun. *Phys. Chem. Chem. Phys.* 2011, **13**, 6205–6210.
33 L. M. Qiu, F. Liu, L. Z. Zhao, Y. Ma and J. N. Yao, *Appl. Surf. Sci.* 2006, **252**, 4931–4935.
34 F. Larachia, J. Pierre, A. Adnot and A. Bernis, *Appl. Surf. Sci.* 2002, **195**, 236–250.
35 S. S. Pan, C. Ye, and G. H. Li, *J. Appl. Phys*. 2006, **100**, 053507.
36 X. M. Teng and H. T, *J. Appl. Phys*. 2010, **107**, 074302.
37 M. Kruk and M. Jaroniec, *Chem. Mater.* 2001, **13**, 3169–3183.
38 Y. C. Qiu, W. Chen and S. H. Yang, *J. Mater. Chem*. 2010, **20**, 1001–1006.
39 L. Matějováa, K. Kǒcíb, M. Relib, A.Hospodkováe and A. Kotarbag, *Appl. Catal. B-Environ.* 2014, **152–153**, 172–183.
40 N. Ökte, *Appl. Catal. A-Gen.* 2014, **475**, 27–39.
41 T. Y. Ma, J. L. Cao, G. S. Shao, X. J. Zhang and Z.Y. Yuan, *J. Phys. Chem. C* 2009, **113**, 16658–16667.
42 G. Xiao, X. Huang, X. P. Liao, and B. Shi, *J. Phys. Chem. C* 2013, **117**, 9739–9746.
43 H. X. Shi, T. Y. Zhang, T. C. An, B. Li and X. Wang, *J. Colloid. Interf. Sci.* 2012, **380,** 121–127.
44 H. W. Huang, K. Liu, K. Chen, Y. L. Zhang, Y. H. Zhang and S. C. Wang, *J. Phys. Chem. C*., 2014, **118**, 14379−14387.
45 N. Tian, Y. H. Zhang, and H. W. Huang, *J. Phys. Chem. C*., 2014, **118**, 15640−15648.
46 P. P. Sun, L. Liu and S. C. Cui, *Catal. Lett*. 2014, **144**, 2107–2113.
47 A. K. L. Sajjad, S. Shamaila, B. Tian, F. Chen and J. Zhang, *Appl. Catal. B*. 2009, **91**, 397–405.
48 C. X. Xu, G. P. Zhu, X. Li, Y. Yang, S. T. Tan, X. W. Sun, C. Lincoln and T. A. Smith, *J. Appl. Phys*. 2008, **103,** 094303.
49 Q. J. Yu, W. Y. Fu, C. L. Yu, H. B. Yang, R. H. Wei, M. H. Li and S .K. Liu, *J. Phys. Chem. C*. 2007, **111,** 17521.
50 S. Bagwasi, Y. Niu, M. Nasir, B. Tian and J. Zhang, Appl. *Surf. Sci.* 2013, **264**, 139–147.
51 C. J. Chang, C. Y. Lin and M. H. Hsu, *J. Taiwan. Inst. Chem. E.* 2014, **45,** 1954–1963.

52 M. Nasir, J. L. Zhang, F. Chen and B. Z. Tian, *Res. Chem. Intermed*. 2015, **41**, 1607–1624.
53 J. M. Coronado, A. J. Maira, A. Martinez-Arias, J. C. Conesa and J. Soria, *J. Photochem. Photobiol. A* 2002, **150**, 213–221.

Graphical Abstract

Porous 3D Ce-doped ZnO microflowers were fabricated by using low temperature-hydrothermal method followed by a heat treatment process for the first time. Such the unique porous 3D structure of Ce-doped ZnO composites displays excellent photocatalytic activity on degradation of Rhodamine B. And the composite of Ce-doped ZnO is a promising candidate material for future treatment of contaminated water.